

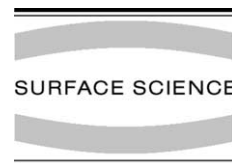


ELSEVIER

Available online at [www.sciencedirect.com](http://www.sciencedirect.com)

SCIENCE @ DIRECT®

Surface Science 531 (2003) 287–294



[www.elsevier.com/locate/susc](http://www.elsevier.com/locate/susc)

# Growth and oxidation of a Ni<sub>3</sub>Al alloy on Ni(1 0 0)

A. Wehner \*, Y. Jelizova, R. Franchy

*Institut für Schichten und Grenzflächen (ISG 3) Forschungszentrum Jülich D-52425, Germany*

Received 18 December 2002; accepted for publication 11 March 2003

## Abstract

The growth and oxidation of a thin film of Ni<sub>3</sub>Al grown on Ni(1 0 0) were studied using Auger electron spectroscopy (AES), low energy electron diffraction (LEED), and high resolution electron energy loss spectroscopy (EELS). At 300 K, a 12 Å thick layer of aluminium was deposited on a Ni(1 0 0) surface and subsequently annealed to 1150 K resulting in a thin film of Ni<sub>3</sub>Al which grows with the (1 0 0) plane parallel to the (1 0 0) surface of the substrate. Oxidation at 300 K of Ni<sub>3</sub>Al/Ni(1 0 0) until saturation leads to the growth of an aluminium oxide layer consisting of different alumina phases. By annealing up to 1000 K, a well ordered film of the Al<sub>2</sub>O<sub>3</sub> film is formed which exhibits in the EEL spectra Fuchs–Kliwer phonons at 420, 640 and 880 cm<sup>-1</sup>. The LEED pattern of the oxide shows a twelfold ring structure. This LEED pattern is explained by two domains with hexagonal structure which are rotated by 90° with respect to each other. The lattice constant of the hexagonal structure amounts to ~2.87 Å. The EELS data and the LEED pattern suggest that the γ'-Al<sub>2</sub>O<sub>3</sub> phase is formed which grows with the (1 1 1) plane parallel to the Ni(1 0 0) surface.

© 2003 Elsevier Science B.V. All rights reserved.

*Keywords:* Nickel; Aluminum oxide; Alloys; Oxidation; Growth; Low energy electron diffraction (LEED)

## 1. Introduction

Intermetallic alloys have gained much interest because of their physical and mechanical properties, like high melting point, low density, and good corrosion resistance. Some possible applications of intermetallics, e.g. in areas of energy storage and furnace hardware, have been reviewed by Stoloff et al. [1]. Also, thin films of metals and intermetallics are intensively studied, because, due to the low dimensionality, they have some interesting properties different from those of the bulk. Thin

films of Al<sub>2</sub>O<sub>3</sub> are utilized in different fields of applications as catalysis [2] and microelectronics and are also used as insulating barrier in magnetic tunnel junctions [3]. In general, the controlled epitaxial growth of ultrathin oxide (Al<sub>2</sub>O<sub>3</sub>, Ga<sub>2</sub>O<sub>3</sub>) layers on ferromagnetic substrates with a well defined ferromagnet/insulator interface is of crucial importance for the understanding of the spin-dependent tunnelling. Therefore, many attempts are done to find procedures to grow well defined homogenous oxide layers with a thickness in the range of few tens of Å. Recently, tunnel magneto resistance (TMR) amplitudes of more than 40% at room temperature have been achieved [4].

The growth of thin films of aluminium oxides on metals and metal alloys has recently been reviewed by Franchy [5]. In general, upon oxidation of the

\* Corresponding author. Tel.: +49-2461-614633; fax: +49-2461-613907.

E-mail address: [a.wehner@fz-juelich.de](mailto:a.wehner@fz-juelich.de) (A. Wehner).

surface of a NiAl compound a thin film of  $\text{Al}_2\text{O}_3$  is grown [6–12], whereas in most studies in UHV no evidence for the oxidation of Ni was found [7,12,13]. Well ordered, ultrathin  $\text{Al}_2\text{O}_3$  films have been prepared at 700–1200 K on  $\text{Ni}_3\text{Al}(111)$  [7, 14],  $\text{Ni}_3\text{Al}(100)$  [9,15],  $\text{NiAl}(111)$  [10],  $\text{NiAl}(110)$  [12], and  $\text{NiAl}(100)$  [11]. The preparation of  $\text{Al}_2\text{O}_3$  films was also studied on pure aluminum [16],  $\text{Ru}(0001)$  [17] and  $\text{Mo}(110)$  [18]. The advantage of preparing  $\text{Al}_2\text{O}_3$  on surfaces of NiAl alloys is that these substrates have a high melting temperature which allows the formation of well ordered (crystalline) ultrathin oxide layers.

$\text{Al}_2\text{O}_3$  exists in different phases, all of which are based on a close-packed oxygen lattice [19] in which the  $\text{Al}^{3+}$  cations occupy tetrahedral and/or octahedral sites. Differences in occupation probability of these sites determine the crystal structure. For example, the amorphous alumina can be described as clusters of close-packed oxygen with Al ions sitting only in tetrahedral vacancies [20], while  $\gamma$ - and  $\gamma'$ - $\text{Al}_2\text{O}_3$  have a cubic spinel structure with Al ions in tetrahedral and octahedral positions.

By deposition and subsequent annealing at 820 K of one monolayer (ML) Al on a  $\text{Ni}(100)$  surface Lu et al. [21] and O'Connor et al. [22] have prepared a thin layer of  $\text{Ni}_3\text{Al}$ . The thin film of  $\text{Ni}_3\text{Al}$  grows with the (100) plane parallel to the (100) surface of  $\text{Ni}(100)$ . The surface structure of the  $\text{Ni}_3\text{Al}/\text{Ni}(100)$  was investigated by low energy electron diffraction (LEED) [21,22] and ion scattering [22]. Deposition of Al at 520 K on  $\text{Ni}(100)$  also leads to the formation of  $\text{Ni}_3\text{Al}$  [21].

In this paper we report on the preparation of a thin film of  $\text{Al}_2\text{O}_3$  which was grown by oxidation of a  $\text{Ni}_3\text{Al}(100)$  thin layer grown on  $\text{Ni}(100)$ . Oxidation at 300 K of  $\text{Ni}_3\text{Al}/\text{Ni}(100)$  leads to the formation of an oxide film consisting of a mixture of different  $\text{Al}_2\text{O}_3$  phases (amorphous and unorderd). By annealing up to 1200 K a well ordered thin film of  $\gamma'$ - $\text{Al}_2\text{O}_3$  is formed. The paper is organized as follows: Section 2 presents the experimental conditions and the cleaning procedure of the sample. Section 3.1 deals with the growth of a thin  $\text{Ni}_3\text{Al}$  layer on  $\text{Ni}(100)$ . The oxidation of  $\text{Ni}_3\text{Al}$  is described in Section 3.2. Section 3.3 presents the formation of a well-ordered  $\gamma'$ - $\text{Al}_2\text{O}_3$  film

on  $\text{Ni}(100)$ . In section 4 some conclusions are summarized.

## 2. Experimental

The experiments were performed in a two level ultra-high vacuum (UHV) chamber with a base pressure of about  $4 \times 10^{-8}$  Pa. The upper level is equipped with a cylindrical mirror analyzer (CMA) for Auger electron spectroscopy (AES), a three grid LEED optics, an ion gun, and a quadrupole mass spectrometer (QMS). Auger spectra were recorded in the N(E) mode at a primary energy of 4 keV and the  $dN(E)/dE$  spectra are obtained by numerical differentiation. The LEED images were recorded with a digital camera (Kodak DC290) at an exposure time of typically 16 s. The lower level of the UHV chamber contains a computer controlled high resolution electron energy loss spectrometer (EELS) which is based on the  $127^\circ$  cylindrical deflector [23]. EEL spectra were taken in specular direction at room temperature.

The  $\text{Ni}(100)$  single crystal has a diameter of 8 mm and a thickness of 2.5 mm. The surface was polished mechanically, and the crystal orientation has an accuracy of  $0.5^\circ$ . In UHV, the cleaning of  $\text{Ni}(100)$  was performed by repeated cycles of sputtering ( $\text{Ar}^+$  ions, 1 keV/0.8  $\mu\text{A}$ ) and annealing to 1200 K. Carbon was removed by oxidation at 1000 K and subsequent annealing at 1200 K. The clean  $\text{Ni}(100)$  surface exhibits a sharp ( $1 \times 1$ ) LEED pattern.

Al was evaporated from a crucible filled with pestled crystals of NiAl. The calibration of the Al evaporator was performed with a quartz microbalance. In our experiments a deposition rate of  $r = 0.48 \text{ \AA}/\text{min}$  was used. Oxidation was performed by backfilling the chamber with  $\text{O}_2^{16}$  at partial pressures varying between  $1 \times 10^{-5}$  and  $1 \times 10^{-4}$  Pa. Oxygen exposures are expressed in Langmuirs ( $1 \text{ L} = 1.33 \times 10^{-4} \text{ Pa} \times 1 \text{ s}$ ). Annealing of the sample was performed by electron impact, and the temperature was measured via a W–Re thermocouple which was mounted on the backside of the sample.

Thin films of  $\text{Ni}_3\text{Al}$  and finally  $\text{Al}_2\text{O}_3$  on  $\text{Ni}(100)$  were prepared in the way indicated in Fig. 1:

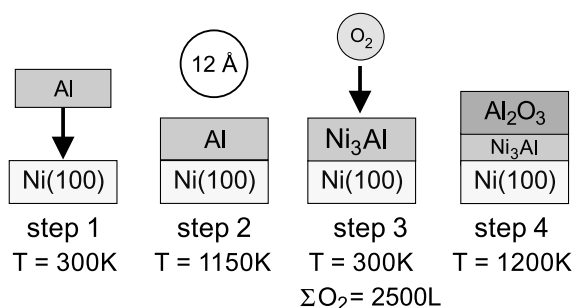


Fig. 1. Schematic illustration of the preparation process. Step 1 represents the deposition of Al on Ni(100), step 2 the annealing from room temperature to 800 K in steps of 100 K and from 800 to 1150 K in steps of 50 K. During annealing the  $\text{Ni}_3\text{Al}$  alloy is formed. Step 3 is the oxidation at 300 K of the  $\text{Ni}_3\text{Al}$  layer, and step 4 represents the annealing of the oxide from room temperature to 1200 K in steps of 100 K.

- *Step 1:* 12 Å of Al are deposited at room temperature on the Ni(100) surface.
- *Step 2:* The system Al/Ni(100) is annealed to 800 K in steps of 100 K, afterwards to 1150 K in steps of 50 K. During annealing a  $\text{Ni}_3\text{Al}$  layer is formed. Each step lasted for 2 min.
- *Step 3:* The system  $\text{Ni}_3\text{Al}/\text{Ni}(100)$  is oxidized at room temperature with oxygen to a total exposure of 2500 L. By oxidation a thin film of  $\text{Al}_2\text{O}_3$  is formed.
- *Step 4:* The system  $\text{Al}_2\text{O}_3/\text{Ni}_3\text{Al}/\text{Ni}(100)$  is annealed to 1200 K in steps of 100 K. By annealing up to 1200 K a well-ordered  $\gamma'$ - $\text{Al}_2\text{O}_3$  phase is formed. Each annealing step lasted for 2 min.

### 3. Results and discussion

#### 3.1. Formation of $\text{Ni}_3\text{Al}$

Fig. 2a shows the p-to-p (peak-to-peak) amplitude of the KLL AES transition of aluminium at 1396 eV as a function of the deposition time. The exact shape of this curve depends of course on the growth mode of aluminium on Ni(100). However, independent of the growth mode, a saturation of the Al signal is reached, when the thickness of the layer exceeds the mean free path of the electrons at the energy of the respective AES transition. Electrons with an energy of 1396 eV (Al, KLL) have a

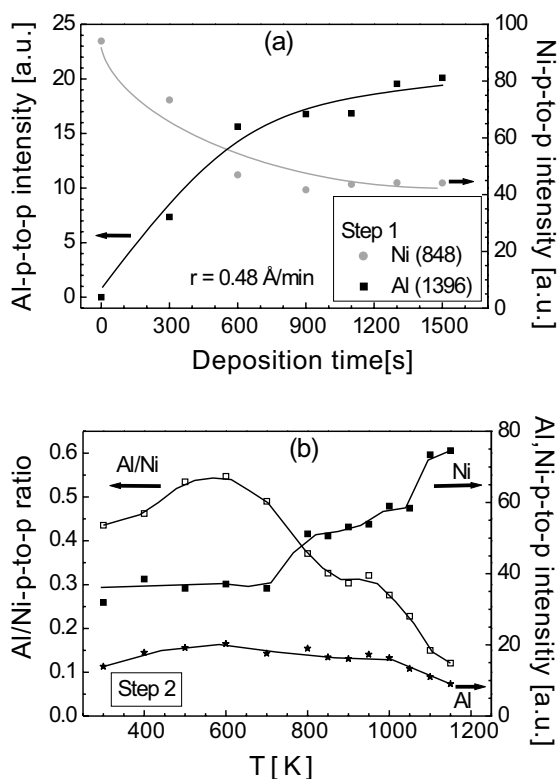


Fig. 2. Part (a) shows the peak-to-peak (p-to-p) intensity in arbitrary units (a.u.) of the AES transition of Al at 1396 eV (left axis) and Ni at 848 eV (right axis) as a function of the deposition time. Part (b) shows the p-to-p intensities of the Al transition at 1396 eV (right axis) and the Ni transition at 848 eV (right axis) as a function of the annealing temperature. Also shown is the p-to-p ratio  $\text{Al}_{1396}/\text{Ni}_{848}$  (left axis).

mean free path of about 24 Å [24] in aluminium. Thus, at this thickness the intensity of the Auger transition should show a saturation level. In our case only 12 Å were deposited and consequently no saturation is reached as can be seen in Fig. 2a. After a deposition time of 1500 s and a deposition rate of 0.48 Å/min the thickness of the Al layer amounts to 12 Å.

Fig. 2b shows the p-to-p intensities of the Ni LMM transition at 848 eV, the Al KLL transition at 1396 eV and the ratio Al/Ni as a function of the annealing temperature. Up to 700 K, the p-to-p intensity of the Ni transition does not change significantly, while above 700 K the signal increases continuously. The increase of the Al intensity and

the ratio Al/Ni in the region from 300 K to  $\sim 600$  K might be due to structural changes and ordering of the Al layer. For  $T \geq 700$  K, the ratio Al/Ni decreases due to the increase of the Ni signal. This suggests that the interdiffusion (alloying) of Ni and Al atoms sets in. After annealing to 1150 K the ratio of Al/Ni corresponds to the ratio of Al/Ni in bulk  $\text{Ni}_3\text{Al}$ . After annealing to 1200 K (not shown) the intensity of the Al transition is close to zero. At this stage the aluminium is most likely completely diffused into the bulk.

Fig. 3 shows: (a) a LEED pattern of the clean Ni(100) surface and (b) a LEED image of the

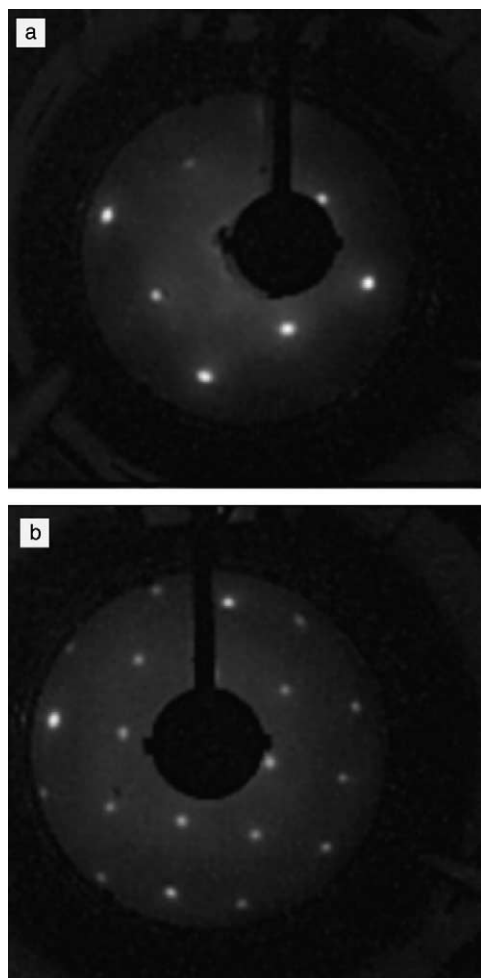


Fig. 3. (a) LEED pattern of the clean Ni(100) surface. (b) LEED image of the  $\text{Ni}_3\text{Al}$  layer. The primary energy of the electrons was 122 eV for both of the images.

sample after annealing to 1150 K of a 12 Å thick Al film on Ni(100). After annealing, the surface exhibits a  $c(2 \times 2)$  structure with respect to the Ni(100) surface. The unit cell is quadratic with a lattice constant of  $(3.52 \pm 0.1)$  Å. This unit cell corresponds to that which is expected for the  $\text{Ni}_3\text{Al}(100)$  surface. This strongly suggests, that on Ni(100) a surface alloy of  $\text{Ni}_3\text{Al}$  is formed. The LEED pattern is in agreement with that found by Lu et al. [21] and O'Connor et al. [22] who have grown a layer of  $\text{Ni}_3\text{Al}$  on Ni(100) by depositing approximately 1 ML of Al onto the Ni(100) surface and annealing at 820 K for 5 min. Although in our case higher annealing temperatures were necessary to obtain an ordered LEED pattern, the LEED pattern and the AES data are clear evidences for the existence of  $\text{Ni}_3\text{Al}$ .

From our experiments we cannot determine the thickness of the  $\text{Ni}_3\text{Al}$  layer strictly. However, we can give an upper limit. The upper limit results from the fact that if the a 12 Å thick Al layer is completely used to form  $\text{Ni}_3\text{Al}$ , then the total number of layers can be calculated from the lattice constant of  $\text{Ni}_3\text{Al}$  and the thickness amounts to about 35 Å.

### 3.2. Oxidation of $\text{Ni}_3\text{Al}(100)/\text{Ni}(100)$

In order to grow a thin aluminum oxide the surface of  $\text{Ni}_3\text{Al}(100)/\text{Ni}(100)$  was oxidized at room temperature. Fig. 4 shows the AES p-to-p ratios  $\text{O}/\text{Ni}_{(848 \text{ eV})}$  and  $\text{O}/\text{Al}_{(1396 \text{ eV})}$  as a function of oxygen exposure (Fig. 1, step 3). The O/Al and O/Ni ratios increase strongly up to 200 L and above 500 L both of the ratios clearly indicate that a saturation is reached. The saturation value ( $\sim 6.5$ ) of the O/Al ratio is approximately the same as for bulk  $\text{Al}_2\text{O}_3$  [25]. We now focus on the AES spectra in Fig. 5, which trace the emergence of Al and  $\text{Al}^{3+}$  transition in the energy region between 10 and 120 eV. Spectrum a shows the spectrum of the clean Ni(100) surface and accordingly two characteristic transitions at 61 and 102 eV occur. The situation after the deposition of a 12 Å thick Al layer is shown in spectrum b. The Ni-transitions at 61 eV and at 102 eV are disappeared and a transition at 68 eV is emerged, which corresponds to the LMM transition of Al. The disappearing of the Ni tran-

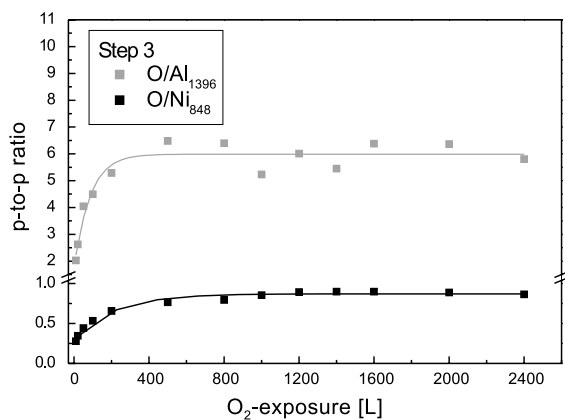


Fig. 4. Peak-to-peak ratios of the AES signal of O/Ni and O/Al during oxidation at 300 K (step 3). Both of the ratios indicate a saturation and the value of the O/Al ratio corresponds to that of bulk  $\text{Al}_2\text{O}_3$  [25].

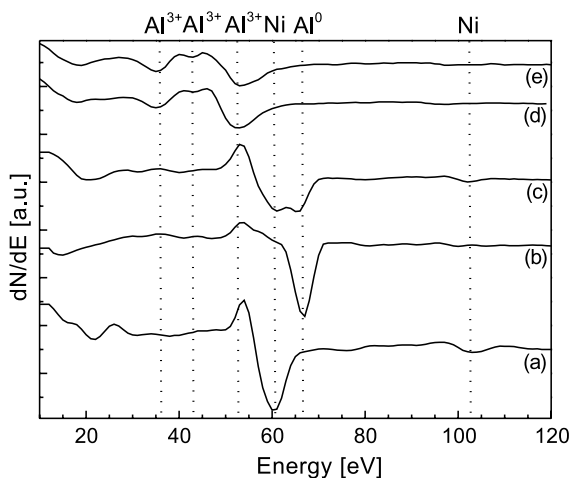


Fig. 5. AES spectra in the energy region between 10 and 120 eV. (a) clean Ni(1 0 0) surface, (b) after deposition of Al (step 1), (c) after annealing to 1200 K (step 2), (d) after oxidation of  $\text{Ni}_3\text{Al}$  at 300 K (step 3), (e) after annealing of the oxide layer at 1200 K (step 4).

sitions is expected, because the mean free path of electrons in this energy region is only few Å, which is much smaller than the Al layer thickness of 12 Å. Maybe some amount of Ni is also evaporated from the pitted NiAl crystals, but the total amount is below the detection limit of AES. After annealing the sample to 1150 K, the transition at 102 eV reemerges and two transitions at 61 eV (Ni,

MNN) and 68 eV (Al, LMM) are clearly resolved (see spectrum c). These facts indicate the reappearance of Ni in the first few layers. After oxidation of the sample to saturation at 300 K only the transitions at 51, 43 and 35 eV occur (spectrum d), which are typical for the formation of  $\text{Al}^{3+}$  [25]. Summarized this is strong evidence for the oxidation of Al, whereas Ni atoms seem to be not involved. In UPS investigations of NiAl [12],  $\text{Ni}_3\text{Al}$  [7] and FeAl [26] it was found that only the Al atoms are oxidized. In our investigation AES is not sensitive enough to rule out completely the Ni-O interactions. Maybe the Ni MNN transition at 61 eV overlaps with the strong signal of the  $\text{Al}^{3+}$  transition at 51 eV, which is observed by the very broad line shape at around 51 eV. The oxidation process can be described as follows: adsorption of oxygen induces the segregation of Al atoms to the surface where by reaction with the adsorbed oxygen an aluminium oxide film is formed. This process is the so called “preferential segregation oxidation” of intermetallic alloys which have Al (or Ga) as a component [5]. Generally, the oxidation of Al is thermodynamically favored over the oxidation of Ni, because the heat of formation of  $\text{Al}_2\text{O}_3$  is much larger ( $\Delta H_f = -1676$  kJ/mol) than that of NiO ( $\Delta H_f = -240$  kJ/mol) [27]. Finally, we give a rough estimate of the thickness of the oxide layer. Assuming that a pure  $\text{Al}_2\text{O}_3$  layer is grown that contains no Ni, the thickness can be determined by the exponential decrease of the intensity of the Ni AES transition at 848 eV. The inelastic mean free path (IMFP) of electrons with energy 848 eV in  $\text{Al}_2\text{O}_3$  was calculated to be 18 Å [28]. The thickness of the  $\text{Al}_2\text{O}_3$  layer amounts to  $d = (11 \pm 2)$  Å. It was found that the thickness of an Al layer is increased by oxidation. For example, Chen et al. claimed that the thickness of Al-oxide is nearly double of the Al film [29]. By assuming that in our case a similar increase takes place, a pure Al film of  $\sim 5.5$  Å would be needed to grow a 11 Å thick layer of  $\text{Al}_2\text{O}_3$ . This is about one half of the initially deposited amount of Al. However, we have to mention that this consideration is valid only for a pure Al layer and not for the oxidation of an intermetallic alloy like  $\text{Ni}_3\text{Al}$ . In principle, it should be possible to trace the oxidation of Al by the KLL AES-transition of metallic Al (1396 eV)

and  $\text{Al}^{3+}$  (1378 eV) [25]. However, during oxidation only a broadening of the transition is observed, which indicates a coexistence of  $\text{Al}^0$  and  $\text{Al}^{3+}$ . Since in spectrum d of Fig. 5 there is no hint of  $\text{Al}^0$  it appears likely, that  $\text{Al}^0$  atoms are not within the topmost 5 Å of the film. Whether the unoxidized Al is in the film or in an interface layer between the Ni(100) substrate and the  $\text{Al}_2\text{O}_3$  film cannot be determined.

### 3.3. Annealing of the oxide

The vibrational properties of the  $\text{Al}_2\text{O}_3$  film on  $\text{Ni}_3\text{Al}/\text{Ni}(100)$  were investigated by EELS. Fig. 6 shows EEL spectra of the sample during annealing of the oxide. The spectrum at the bottom was recorded after oxidation at 300 K (saturation) and exhibits three broad losses at about 420, 620, and 860  $\text{cm}^{-1}$ . After annealing to 1200 K, the losses at 620 and 860  $\text{cm}^{-1}$  are shifted to 640 and 880  $\text{cm}^{-1}$ . For an amorphous  $\text{Al}_2\text{O}_3$  (*a*- $\text{Al}_2\text{O}_3$ ) only two IR active modes are expected [5], because the  $\text{Al}^{3+}$  ions occupy exclusively tetrahedral sites [20,30]. The fact that already at room temperature three losses are observed indicates, that even at room temperature both tetrahedral and octahedral sites of the  $\text{O}^{2-}$  lattice are occupied by  $\text{Al}^{3+}$  ions (see e.g. [5] and references therein). Thus, at 300 K the

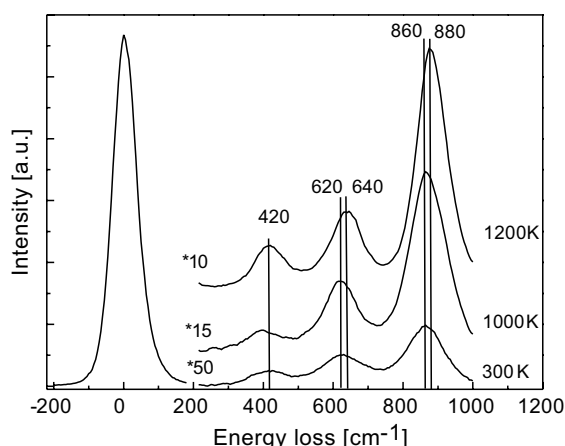


Fig. 6. EEL spectra taken during annealing of the oxide layer. After annealing to 1200 K, the frequency of the losses originally at 620 and 860 are shifted to 640 and 880  $\text{cm}^{-1}$ , respectively.

grown  $\text{Al}_2\text{O}_3$  film does not only consist of an amorphous phase, but rather of a mixture of different  $\text{Al}_2\text{O}_3$  phases. This assumption is supported by the LEED pattern, which is diffuse due to the lack of a long-range order. Between room temperature and 700 K the EEL spectra do not change significantly. Upon annealing above 800 K, the intensity of the losses (the magnification factor of the losses decreases from 50 at 300 K to 10 after annealing at 1200 K) and of the elastic beam increase, indicating that an ordering of the oxide layer takes place. The spectra after annealing to 1000 and 1200 K are shown in Fig. 6 and exhibit losses at 420, 640 and 880  $\text{cm}^{-1}$ . EEL spectra of thin well-ordered alumina films ( $\gamma$ -,  $\gamma'$ - and  $\theta$ - $\text{Al}_2\text{O}_3$ ) on metal and metal alloy surfaces show commonly three (sometimes four) distinct phonon features in the frequency regions of 380–430, 620–660, and 850–990  $\text{cm}^{-1}$  with slightly different relative loss intensities between the modes (Ref. [5] and the references therein). Therefore, we conclude that in the case of  $\text{Al}_2\text{O}_3$  on Ni(100) the Al oxide belongs to an ordered  $\text{Al}_2\text{O}_3$  phase. The increase of ordering is in accordance with the emergence of Bragg reflections in the LEED images at 900 K. 1200 K seems to be the temperature where the oxide got the best ordering. However, we have to mention that the unoxidized  $\text{Ni}_3\text{Al}$  layer on Ni(100) is destroyed at around 1200 K and may be this is at least in part also the case after annealing the oxide covered  $\text{Ni}_3\text{Al}$  layer. Unfortunately, no evidences on the hidden interfaces  $\text{Al}_2\text{O}_3/\text{Ni}_3\text{Al}$  and  $\text{Ni}_3\text{Al}/\text{Ni}(100)$  are available in our experiment.

Spectrum e in Fig. 5 shows an AES spectrum of the oxide layer in the energy range between 10 and 120 eV after annealing to 1200 K. This spectrum is similar spectrum d, which suggests that during annealing no change of the ionicity of the Al develops.

Fig. 7(a) shows a LEED pattern of the sample taken after annealing the oxide to 1200 K and (b) shows a schematic representation of the pattern. A twelfold ring structure is observed which results from two domains with hexagonal structure which are rotated with an angle of  $n \cdot 30^\circ$  ( $n$  odd) with respect to each other. Because of the square lattice ( $C_4$  symmetry) of the substrate it appears reason-

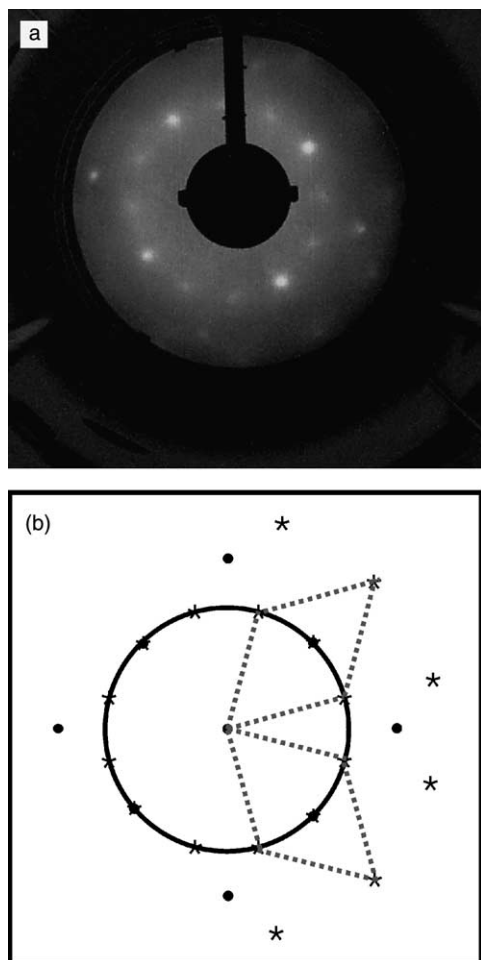


Fig. 7. (a) LEED image of the oxide after annealing at 1200 K. The primary energy was 122 eV. (b) schematic representation: substrate spots are indicated by dots, spots stemming from the oxide are indicated by asterisks.

able to assume an angle of rotation of  $90^\circ$ . From the half width of the spots the diameter of the domains is estimated to be about  $30 \text{ \AA}$ . In order to determine the structure of the  $\text{Al}_2\text{O}_3$  film we have to consider again the EELS data. The three losses in the EEL spectra clearly rule out the existence of  $\alpha\text{-Al}_2\text{O}_3$  [31], because in  $\alpha\text{-Al}_2\text{O}_3$  the  $\text{Al}^{3+}$  ions occupy only octahedral sites which induce only two IR active modes and not three. Therefore the observed hexagonal structure has to be explained by a (111) plane of a cubic  $\text{Al}_2\text{O}_3$  phase which grows with the (111) plane of the oxide parallel to

the (100) plane of the Ni substrate. The lattice constant of the hexagonal unit cell was determined to be  $a_{\text{hex}} = (2.87 \pm 0.2) \text{ \AA}$ . This agrees with the distance between two adjacent  $\text{O}^{2-}$  ions in the (111) plane of a number of cubic phases of  $\text{Al}_2\text{O}_3$  [32]. From the agreement of the EELS [9] and LEED [7,9] data obtained for the oxidation of  $\text{Ni}_3\text{Al}$  single crystal surfaces with those of this study, the growth of the  $\gamma\text{-Al}_2\text{O}_3$  phase is concluded, which grows with the (111) surface parallel to the Ni(100) surface. The thickness of the  $\text{Al}_2\text{O}_3$  film after annealing to 1200 K amounts to  $(8 \pm 2) \text{ \AA}$ .

Fig. 8 shows the ratio of the peak to peak intensities of O/Al as a function of the annealing temperature of the oxide. Since the value of this ratio does not change significantly it appears reasonable to assume that the stoichiometry does not change during annealing. From this ratio together with the relative Auger sensitivities the ratio between the aluminium and oxygen ions in the  $\text{Al}_2\text{O}_3$  layer can be estimated. The ratio is determined to be 6.2, by using the relative sensitivity of 0.4 for the oxygen transition and 0.09 for the aluminium transition [33]. Therefore the ratio between the amount of O and Al ions in the oxide layer is  $\sim 1.4$  which is close to the value of 1.5 of  $\text{Al}_2\text{O}_3$ . The discrepancy can be assigned to the experimental inaccuracy.

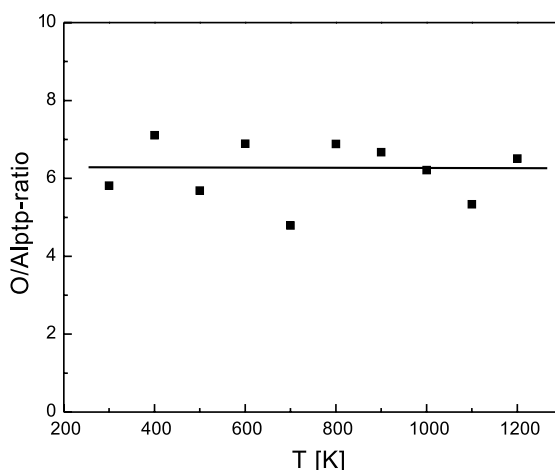


Fig. 8. The peak-to-peak ratio of O/Al during annealing of the oxide. The horizontal line is a guide to the eye.

#### 4. Conclusion

In conclusion, upon deposition and annealing of Al on a Ni(100) surface, a thin layer of Ni<sub>3</sub>Al is formed. Exposing the surface of this alloy to oxygen and subsequent annealing, leads to the formation of Al<sub>2</sub>O<sub>3</sub>. At 300 K the thickness of the Al<sub>2</sub>O<sub>3</sub> layer is approximately  $(11 \pm 2)$  Å, which changes to  $(8 \pm 2)$  Å after annealing to 1200 K.

After annealing up to 1200 K, the aluminium oxide shows a sharp LEED image with a twelve-fold ring structure, indicating long range order and a hexagonal structure of two domains which are rotated by 90° with respect to each other. The oxide grows with the (111) plane of the  $\gamma'$ -Al<sub>2</sub>O<sub>3</sub> lattice parallel to the (100) plane of the Ni substrate. The lattice constant of the hexagonal unit cell was determined to be  $\sim 2.87$  Å.

#### Acknowledgements

This work was supported by the HGF project “Magnetoelectronics” and represents a part of the PhD work of A.W. at the Heinrich Heine Universität Düsseldorf, Germany.

#### References

- [1] N.S. Stoloff, C.T. Liu, S.C. Deevi, *Intermetallics* 8 (2000) 1313.
- [2] H.J. Freund, E. Umbach, *Adsorption on ordered Surfaces of Ionic Solids and Thin Films*, Springer, Heidelberg, 1993.
- [3] J.S. Moodera, L.R. Kinder, *J. Appl. Phys.* 79 (1996) 4724.
- [4] S.S. Parkin et al., *JAP* 85 (1999) 5828.
- [5] R. Franchy, *Surf. Sci. Rep.* 38 (2000) 195.
- [6] Y.G. Shen, D.J. O'Connor, R.J. MacDonald, *Surf. Interface Anal.* 17 (1991) 903.
- [7] U. Bardi, A. Atrei, G. Rovida, *Surf. Sci.* 268 (1992) 87.
- [8] G.F. Cotterill, H. Niehus, D.J. O'Connor, *Surf. Rev. Lett.* 3 (1996) 1355.
- [9] V. Podgursky, I. Costina, R. Franchy, *Appl. Surf. Sci.* 206 (2003) 29.
- [10] R. Franchy, J. Masuch, P. Gassmann, *Appl. Surf. Sci.* 93 (1996) 317.
- [11] P. Gassmann, R. Franchy, H. Ibach, *Surf. Sci.* 319 (1994) 95–109.
- [12] M. Jaeger, K. Kuhlenbeck, H.J. Freund, M. Wuttig, W. Hoffmann, R. Franchy, H. Ibach, *Surf. Sci.* 259 (1991) 235.
- [13] A. Venezia, C. Loxton, *Surf. Sci.* 194 (1988) 136.
- [14] C. Becker, J. Kandler, H. Raaf, R. Linke, T. Pelster, M. Draeger, M. Tanemura, K. Wandelt, *J. Vac. Sci. Technol. A* 16 (1998) 1000.
- [15] I. Costina, PhD-Thesis. Duesseldorf: Heinrich-Heine-Universität, 2002.
- [16] J.L. Erskine, R.L. Strong, *Phys. Rev. B* 25 (1982) 5547.
- [17] M.B. Lee, J.H. Lee, B.G. Frederick, N.V. Richardson, *Surf. Sci.* 448 (2000) L207.
- [18] P.J. Chen, M.L. Colaianni, J.T. Yates Jr., *Phys. Rev. B* 41 (1990) 8025.
- [19] H. Jagodzinski, *Z. Krist.* 109 (1957) 388.
- [20] R. Manaila, A. Dévényi, E. Candet, *Thin Solid Films* 122 (1984) 131.
- [21] S.H. Lu, D. Tian, Z.Q. Wang, Y.S. Li, F. Jona, *Solid State Comm.* 67 (1988) 325.
- [22] D.J. O'Connor, M. Draeger, A.M. Molenbroek, Y.G. Shen, *Surf. Sci.* 357–358 (1996) 202.
- [23] H. Ibach, *Electron Energy Loss Spectroscopy—The Technology of High Performance*, Springer, Berlin, 1991.
- [24] S. Tanuma, C.J. Powell, D.R. Penn, *Surf. Interface Anal.* 17 (1991) 911.
- [25] L.E. Davis, N.C. MacDonald, P.W. Palmberg, G.E. Riach, R.E. Weber, *Handbook of Auger Electron Spectroscopy*, Physical Electronics Industries, Eden Prairie, 1976.
- [26] H. Graupner, L. Hammer, K. Heinz, D.M. Zehner, *Surf. Sci.* 380 (1997) 335.
- [27] D.R. Lide, *Handbook of Chemistry and Physics*, CRC Press, 1994.
- [28] S. Tanuma, C.J. Powell, D.R. Penn, *Surf. Interface Anal.* 17 (1991) 927.
- [29] E.Y. Chen, R. Whig, J.M. Slaughter, D. Cronk, J. Goggin, G. Steiner, S. Tehrani, *J. Appl. Phys.* 87 (2000) 6061.
- [30] G. Gutierrez, B. Johansson, *Phys. Rev. B* 65 (2002) 104202.
- [31] M. Liehr, P.A. Thiry, J.J. Pireaux, R. Caudano, *J. Vac. Sci. Technol. A* 2 (1984) 1079.
- [32] H.D. Megaw, *Crystal Structures: A Working Approach*, Sanders, Philadelphia, 1973.
- [33] G. Ertl, J. Küppers, *Low Energy Electrons and Surface Chemistry*, 2nd ed, Weinheim, New York, 1985.